

Simultaneous 3D MR Elastography of the In Vivo Mouse Brain

Steven P. Kearney^{1,3}, Shreyan Majumdar², Thomas J. Royston¹, and Dieter Klatt^{1*}

¹Department of Mechanical and Industrial Engineering, University of Illinois at Chicago, Chicago, IL, USA

²Richard and Loan Hill Department of Bioengineering, University of Illinois at Chicago, Chicago, IL, USA

³Advanced Photon Source, Argonne National Laboratory, Argonne, IL, USA

Steven P. Kearney, Ph.D.

(Previous Address)

Engineering Research Facility (ERF) 2039, 842 W Taylor St.

Department of Mechanical and Industrial Engineering (MC 251)

University of Illinois at Chicago, Chicago, IL 60607

(Current Address)

Argonne National Laboratory Bldg. 401 Rm C1272

9700 S Cass Ave, Argonne, IL 60439

Email: skearney@aps.anl.gov, Phone: (630) 252-7518

Shreyan Majumdar

Clinical Sciences North (CSN) W103, 820 S Wood St.

Department of Bioengineering (MC 563)

University of Illinois at Chicago, Chicago, IL 60612

Email: smajum4@uic.edu,

Thomas J. Royston, Ph.D.

Science and Engineering Offices (SEO) 212, 851 S Morgan St.

Department of Bioengineering (MC 063)

University of Illinois at Chicago, Chicago, IL 60607

Email: troyston@uic.edu, Phone: (312) 996-2335

***Dieter Klatt, Ph.D. (Corresponding Author)**

Clinical Sciences North (CSN) W103, 820 S Wood St.

Department of Bioengineering (MC 563)

University of Illinois at Chicago, Chicago, IL 60612

Email: dklatt@uic.edu, Phone: (312) 413-1747

ABSTRACT:

The feasibility of sample interval modulation (SLIM) magnetic resonance elastography (MRE) for the in vivo mouse brain is assessed, and an alternative SLIM-MRE encoding method is introduced. In SLIM-MRE, the phase accumulation for each motion direction is encoded simultaneously by varying either the start time of the motion encoding gradient (MEG), SLIM-phase constant (SLIM-PC), or the initial phase of the MEG, SLIM-phase varying (SLIM-PV). SLIM-PC provides gradient moment nulling, but the mutual gradient shift necessitates increased echo time (TE). SLIM-PV requires no increased TE, but exhibits non-uniform flow compensation. Comparison was to conventional MRE using six C57BL/6 mice. For SLIM-PC, the Spearman's rank correlation to conventional MRE for the shear storage and loss modulus images were 80% and 76%, respectively, and likewise for SLIM-PV, 73% and 69%, respectively. The results of the Wilcoxon rank sum test showed that there were no statistically significant differences between the spatially averaged shear moduli derived from conventional-MRE, SLIM-PC, and SLIM-PV acquisitions. Both SLIM approaches were comparable to conventional MRE scans with Spearman's rank correlation of 69%-80% and with 3 times reduction in scan time. The SLIM-PC method had the best correlation, and SLIM-PV may be a useful tool in experimental conditions, where both measurement time and T2 relaxation is critical.

Keywords: elastography, SLIM, shear modulus, MRE, stiffness, simultaneous

1. Introduction

Magnetic resonance elastography (MRE), is a phase contrast-based MRI imaging technique that is capable of imaging the spatial distributions of material properties, called elastograms or stiffness maps (Muthupillai *et al.*, 1995). External mechanical vibrations are applied to a material or tissue of interest, and the resulting wave motion is encoded in the phase image using motion encoding gradients (MEGs). The phase image is then processed by an inversion algorithm to produce the elastogram (Oliphant *et al.*, 2001). Contrast in the elastogram is related to variations in the wave field. For example, the wavelengths are longer in a hard tissue than in a soft tissue. This concept has found success as a metric in characterizing pathological tissue changes in, but not limited to, the brain (Wuerfel *et al.*, 2010; Murphy *et al.*, 2011; Freimann *et al.*, 2012; Streitberger *et al.*, 2011), liver (Asbach *et al.*, 2008; Yin *et al.*, 2007; Venkatesh *et al.*, 2008), prostate (Li *et al.*, 2011; Sahebjavaher *et al.*, 2015), pancreas (Shi *et al.*, 2015), breast (Sinkus *et al.*, 2005), heart (Elgeti *et al.*, 2008), and lung (Mariappan *et al.*, 2011).

Much success has been found using MRE as a diagnostic tool for human imaging (Mariappan *et al.*, 2010); for the animal model this is true as well. For instance, many studies have focused on murine models of the brain to assess multiple sclerosis (Schregel *et al.*, 2012), Alzheimer's (Murphy *et al.*, 2012), tumors (Jamin *et al.*, 2015), and traumatic brain injury (Boulet *et al.*, 2013). Of note, MRE is currently the only noninvasive method capable of determining cerebral mechanical properties. Typically, MRE scans are longer than MRI scans due to the multiple time steps used in MRE (especially when acquiring all three motion directions with multiple phase offsets of the propagating wave), and this can increase the possibility of errors due to bulk motion of the animal. In addition, the prolonged duration of anesthesia puts more stress on the animal. Reducing scan times could also have potential benefits for MRE imaging of the torso which requires gating and long scan times.

Currently, there are methods to reduce MRE scan times already in practice. For instance, use of fast imaging pulse sequences such as echo planar imaging (EPI) (Herzka *et al.*, 2009; Sack *et al.*, 2008) or fractional encoding (Rump *et al.*, 2007) have worked well, but at a cost of signal to noise ratio (SNR) or limited phase encoding efficiency. Alternatively, time reduction can be made by assuming that the wave propagation is in plane; therefore, it is necessary to encode only one motion direction, as suggested in (Clayton *et al.*, 2011). However, the degree of validity of this assumption depends on the type of actuator and setup used; therefore, it has become customary, in current MRE implementations, to acquire the full 3D vector field. It has also been shown possible to use multiple imaging methods simultaneously, making more efficient use of total scan time (Yin *et al.*, 2014).

Recently, a novel method to simultaneously encode all three motion directions, called sample interval modulation (SLIM), was developed (Klatt *et al.*, 2013). All three displacement projections are

encoded concurrently by varying the start times of the MEGs relative to the vibration actuation. This method has 3 times reduction in total scan time with a small SNR decrease, which is due to the increase in TE time necessary for MEG start time variation. This technique has been shown to work well in the human brain (Klatt *et al.*, 2015), but has yet to be tested in experimental conditions with shorter T2, such as human liver MRE or pre-clinical MRE at high magnetic field strengths.

The purpose of this study is to assess the feasibility of the SLIM-MRE technique for in vivo mouse brain MRE, and to introduce and assess an alternative SLIM method. The modified SLIM technique works by varying the initial phase of the MEG rather than the MEG start time, thus avoiding the need for echo time (TE) increase but at the cost of non-uniform gradient moment nulling characteristics and this work is related to a framework of MRE sequence design proposed by Nir et al (Nir *et al.*, 2015). Assessment will be based on the similarity of wave and elastogram images of each SLIM method to the ones obtained using conventional MRE. In addition, the spatially averaged shear modulus values will be compared using the Wilcoxon rank sum test to identify any significant variation between methods.

2. Theory

The quantity of phase accumulation ϕ from vibration induced motion, at a frequency f , is the principal equation in MRE, and is given by the time integral of the scalar product of the motion \mathbf{u} and motion encoding gradient (MEG) \mathbf{G} (Klatt *et al.*, 2015):

$$\phi(s) = \gamma \int_s^{s+\tau} \mathbf{G}(t) \cdot \mathbf{u}(t) dt, \quad (1)$$

where γ , s and τ correspond to the gyromagnetic ratio, the start time of the MEG and the duration of MEG application, respectively. Typically, the harmonic component of the measured vibration in the form of a complex phase image Φ after temporal Fourier transform is used as input for inversion of MRE data. Therefore, ϕ is discretized by acquiring N discrete time steps evenly distributed over integer j periods of the vibration frequency (Klatt *et al.*, 2013); enabling the complex-valued phase image Φ to be determined as the j^{th} harmonic after Fourier transform of $\phi(s)$. The discretized solution of Eq. (1) is given by:

$$\phi_n = \phi_0 \cos(\theta_0 - \psi_{nj}), \quad (2)$$

where n is the encoding direction, ϕ_0 , commonly referred to as the encoding efficiency, is a function of gradient strength, vibration frequency, vibration amplitude, and the number of MEG cycles, θ_0 is the

initial phase of the vibration, and ψ_{nj} corresponds to the difference in phase between the MEG and the vibration. Sampling Eq. (2) over j vibration periods,

$$\psi_{nj} = j \frac{2\pi n}{N}, \quad (3)$$

encodes the complex phase image in the j^{th} frequency component. In conventional MRE, the acquisition of the 3D displacement information is separated into three individual temporally-resolved scans for each spatial direction and uses only one frequency bin with $j = 1$ for information storage.

SLIM-MRE makes use of the other frequency components and encodes all spatial directions simultaneously by altering the sampling frequency resulting in a summation of Eq. (2) (Klatt *et al.*, 2015).

$$\phi_n = \phi_0 \sum_{j=1}^3 \cos(\theta_0 - \psi_{nj}) \quad (4)$$

Each direction j can now be sampled at a different rate, and the Fourier transform of Eq. (4) will have each motion direction placed in a separate frequency bin.

In the presented study we use two different approaches for sampling the direction-specific phase differences ψ_{nj} . One of the two approaches, which has already been introduced in previous studies (Klatt *et al.*, 2013; Klatt *et al.*, 2015), varies ψ_{nj} by delaying the start time of MEG components, but keeping their initial phases constant; we will call this method SLIM phase constant (SLIM-PC). The second method, SLIM phase varying (SLIM-PV), varies the start phase of MEG components at their onset and keeps their start times constant. Figure 1 shows the direct comparison of the two methods for 8 time steps. Notice that the SLIM-PC method requires an increase in TE duration due to the mutual gradient shift. On the other hand, SLIM-PV varies between flow compensated gradient shapes and non-flow compensated shapes.

3. Methods

In this study, the techniques of SLIM-PC and SLIM-PV, applied to the in vivo mouse brain, were compared to the conventional MRE acquisitions. Six female C57BL/6 adult mice were used (aged 3 – 8 months), and all experimental procedures were approved by the University of Illinois at Chicago's Institutional Animal Care and Use Committee. MRE scans were performed using an Agilent 9.4 T small animal scanner (Agilent Technologies, Santa Clara, CA) with a 38 mm inside diameter quadrature birdcage RF coil.

Animals were initially anesthetized using 4.0% isoflurane in oxygen until a lack of motor response was observed, and then anesthesia was maintained at a 1.0 – 2.0% mixture throughout the scans. A model 1030 SA animal monitoring system (SA Instruments; Stony Brook, New York) was used to measure body temperature and respiratory function. Body temperature was maintained with warm air circulated from the end of the magnet opposite the sample insertion side.

Shear waves were induced into the brain by a bite bar actuator, Figure 2. The mouse was placed into the actuator by sliding the nose cone back towards the piezo to clear the bite bar. Then the mouse could be placed into the cradle, and once a secure bite was confirmed the nose cone would be slid back over the mouse head. The nose cone, bite bar, and piezo mount were all made from Stereolithography material (Polylactide Resin 4043D, NatureWorks® LLC, Minnetonka, MN) and were printed on a MakerBot 3D printer (MakerBot Replicator 5th Gen., MakerBot® Industries, LLC, Brooklyn, NY). Vibration was induced by a nonmagnetic amplified piezo actuator (APA60S, Cedrat Technologies, Meylan Cedex, France) capable of 50 μm peak to peak displacement for a 10 g load with a resonance at 1,500 Hz.

Each animal underwent five temporally-resolved MRE scans, 3 sequential scans of each direction using conventional MRE, and 1 each of SLIM-PC and SLIM-PV. In addition, a single mouse underwent, on a separate day, two full 3D conventional MRE scans for use as a baseline comparison. All MRE acquisitions were based on a spin echo (SE) pulse sequence. The only difference to the SE sequence is the addition of motion encoding gradients, Figure 1. To scan the entire mouse brain 24-30 slices were used, depending on mouse brain size. Isotropic voxels of 375 μm on a side were acquired with an FOV of 24 x 24 mm and 64 x 64 pixels. The repetition time and echo time were 1000/12.1 ms for conventional MRE and SLIM-PV and 1000/13.5 ms for SLIM-PC. MRE parameters were: 8 motion encoding gradient cycles, 250 mT/m gradient strength, 8 time steps including 180° phase offsets for static phase noise subtraction, 1000 Hz vibration and MEG frequency, and a total scan time of 51 min for conventional MRE and 17 min for each SLIM-MRE approach.

A Fourier transform was applied to the temporal wave images, and the complex waves, representing X, Y, and Z displacements, were then separated from the 2nd, 1st, and 3rd frequency bins, respectively. Next, the complex wave images were 3D spatially filtered with a low pass Butterworth filter with a cut off of 3 pixels and order 3. Subsequently the curl was applied to remove any contribution from compression waves, and the shear modulus was determined by inverting the overdetermined Helmholtz equation 7 in (Manduca *et al.*, 2001). Outliers > 30 kPa and < 50 Pa were excluded from further data analysis. These conservative thresholds are more than 300% beyond the range of cerebral shear modulus values previously reported in the literature (Clayton *et al.*, 2011).

The Spearman's rank correlation coefficient was used as the metric to assess similarity of images. For example, a value of 1 would mean that the compared images were identical. Image correlation was used to assess curled wave field images and shear modulus map images. For the curled wave field images, the correlation was calculated for each phase step acquired using only the real part and then averaged. For the shear modulus maps, correlation was independently calculated for the real and imaginary parts of the shear modulus images.

As an aid in the relative assessment of correlation results additional scans were performed using repeated conventional MRE, SLIM-PC MRE and SLIM-PV MRE imaging of a single mouse which we call the baseline comparison. Using the repeated scans will provide a relative measure for a comparison to assess the variability of the different MRE methods. In addition the SNR was measured for each baseline scan using the magnitude images. SNR was measured as $0.655 * S / \sigma$, S is the mean signal intensity from the mouse brain and σ is the standard deviation of the noise, and the 0.655 constant is to account for the artificial bias induce from all positive noise (ReviseMRI.com, 2017). For these baseline cases since it is the same mouse, in the same position, and imaged using the same scan method it can be assumed that anything less than unity is due to noise alone. Finally, the spatially averaged complex shear moduli of all mice, averaged from a 3-pixel eroded visually segmented ROI of the brain tissue (Klatt *et al.*, 2015), were compared using a pairwise Wilcoxon rank sum test for each method (Daniel, 2004). A failure to reject the null hypothesis (i.e. $p > 0.05$) signifies that the groups can be considered to be from the same continuous distribution and that there are no statistically significant differences between them.

4. Results

For a more meaningful assessment of cross-method comparisons in this study, first a baseline comparison of two follow-up experiments using conventional MRE, SLIM-PC MRE, and SLIM-PV MRE was performed. The results of the baseline comparison can be seen in Table 1. Scan to scan wave image correlation was above 90% for conventional and SLIM-PV MRE, and ranged from 79-97% for SLIM-PC. Scan to scan shear modulus map correlation was less than wave image correlation for all with SLIM-PC having the least correlation at 78%. By comparing magnitude images of these scans and observing no visible shift greater than a voxel it can be determined that this error is mainly due to imaging noise and not misregistration from animal movement. In addition to correlation the SNR of each scan was recorded to rule out any significant variations due solely to an SNR change rather than the encoding method. The SNR for each repeated scan was reported in Table 2. For almost all scans the SNR is stable from 21-24, with just one outlier in the conventional scan phase direction. From Table 1 we can see that the SNR drop had no noticeable effect on the correlation results as compared to the SLIM cases.

Table 3 displays the Spearman's rank correlation for each mouse of the curled wave field images. For SLIM-PC the comparison to conventional ranged from 79-86%, which is within the range of the repeated SLIM-PC scans (79-97%). For SLIM-PV the comparison to conventional ranged from 58-71%, which is lower than the repeated SLIM-PV scans (96-97%). However, even with the lower correlation values for SLIM-PV, visual comparison of images in Figure 3 show that the wave images, post application of the curl (curled wave field), appear similar and the differences in the images seem to be mainly associated with amplitude variations. These amplitude variations are possibly because of simultaneous application of all three gradients.

Comparing the stiffness maps of Figure 4 it can be seen that all methods show the same general features of the mouse brain. However, the amplitude or contrast of the features does appear to be dissimilar. From Table 4, it can be seen that shear modulus maps of the SLIM-PC method are comparable with the baseline result of the complex shear modulus $G^* = G' + iG''$ (76-80% compared to 78-79%, respectively). For SLIM-PV, the correlation drops to 69-73% as compared to the SLIM-PV baseline of 83-87%.

Finally the spatially averaged shear modulus values, Table 5, are assessed. The percent difference errors of the shear modulus compared to conventional MRE results are 1.4 – 4.8%. Figure 5, shows the pair wise Wilcoxon rank sum test for each method. This method gives a good idea of how well SLIM data performs in assessing groups. Both SLIM methods do not reject the null hypothesis with p-values > 0.05 for the shear storage and loss moduli. This suggests that there is no statistically significant difference between data groups obtained using the various methods.

5. Discussion

In this study, we have introduced an alternative methodology for implementing SLIM, called SLIM phase varying, that does not require an increase in echo time to encode all three motion directions simultaneously. Also, both SLIM methods, phase constant and phase varying, were tested for their feasibility for small animal *in vivo* MRE at higher field strengths. Although the SLIM-PC method was previously successfully tested on phantoms (Klatt *et al.*, 2013) and humans (Klatt *et al.*, 2015), the high field (9.4 T) presents a unique challenge in *in vivo* environment with low T2 for the SLIM-PC concept due to the need of mutually shifted gradients that involves TE increase.

The SLIM-PC and SLIM-PV methods both demonstrate similarity to the conventional MRE method. In terms of shear modulus map similarity, the SLIM-PC method comes out on top with higher correlation, which is comparable to the baseline comparison study. However, for spatially averaged shear modulus results the two methods are not significantly discernable. The Wilcoxon rank sum test concluded

that data from conventional acquisitions, SLIM-PC, and SLIM-PV do not reject the null hypothesis and the acquired data can be considered from the same group. This does not necessarily mean that the methods are equivalent only that both SLIM methods have the potential to be used in a clinical study.

The new SLIM method developed in this study, SLIM-PV, has the advantage of no increase in TE time on the cost of non-uniform flow compensation characteristics at different samples. SLIM-PC, on the other hand, required a TE increase of 1.4 ms using our experimental set-up with one interval of the MEG placed on each side of the 180° refocusing pulse. Theoretically, the minimum increase of TE should have only been 0.75 ms, but restrictions from the duration of the 180° refocusing pulse led to the addition of extra delays to ensure the phase of the vibration and post 180° refocusing pulse MEGs were only half a period out of sync as compared to the pre 180° refocusing pulse MEGs. Prolonged TE times involve a decrease in SNR, which is not very significant for animal studies as several MEG cycles are used. Thus the increase in TE relative to the MEG duration becomes less prominent. For instance, in this study 8 cycles of the MEG were used, which had a total duration of 8 ms. The TE increase for SLIM-PC was only 17.5% of the MEG duration. However, human studies use longer vibration periods and less MEG cycles. Thus the TE increase, both the absolute value and the value relative to the MEG duration, may be a more significant factor in SLIM-PC. For the above reasons the SLIM-PV approach may be useful for clinical applications that use spatially averaged mechanical properties as the diagnostic parameter and with experimental conditions where both measurement time and T2 relaxation are critical, such as human liver MRE for assessment of the grade of hepatic fibrosis.

We note that in Table 1 SLIM-PV outperforms SLIM-PC, while in Tables 3 and 4 it is the other way around. The maps of both SLIM-PC and SLIM-PV appear similar to the conventional MRE maps based on visual inspection, but the correlation coefficients in Tables 3 and 4 are better for SLIM-PC than for SLIM-PV. This is likely due to the order in which the scans were performed, which was conventional, then SLIM-PC followed by SLIM-PV. It is our speculation that the longer time interval between SLIM-PV and conventional, as compared to SLIM-PC and conventional, may have resulted in small changes in experimental conditions, such as coupling of the actuator rod and image registration, which then manifested as reduced values of the correlation coefficients. Finally, this did not have influence on the ROI-averaged mechanical properties, which were the same within the error margins of MRE for all three methods.

Comparing the two SLIM approaches to conventional MRE the correlation values were generally lower than the ideal case of comparing two repeated MRE scans. However, even in the repeated scans correlations were still as low as 79% suggesting that there was significant noise to begin with. This study required a total of 5 consecutive scans. Therefore, spatial resolution was kept relatively low to limit the

duration each mouse was anesthetized and in the scanner. At $(375 \mu\text{m})^3$ isotropic voxel resolution a typical wavelength measured only about 8-10 voxels with the vibration frequency of 1 kHz used in this study. This had the effect of making the filter characteristic very sensitive to the cut-off values chosen. For instance, variation of one pixel could change the spatial average as much as ± 1 kPa. So, the cut-off was kept at three pixels to be conservative and this likely resulted in incomplete noise reduction. Future implementation (not comparison studies) of SLIM will not have this problem; as the 2/3 time reduction enabled by SLIM can allow for significantly increased spatial resolution by using the saved time for averaging or longer TR. This will increase the number of voxels within the ROI, which will have a positive effect on the precision of the data.

Even with the low spatial resolution, shear modulus data compared well and are in agreement with previous studies. For instance, McGarry et al. (McGarry *et al.*, 2015) demonstrated mean coefficients of variation for the shear modulus of 14-30% using an advanced iterative inversion algorithm (McGarry *et al.*, 2012), which is comparable to the correlation results found in this study.

Concomitant field terms are always present with nonlinear spatial dependence, when linear gradients are activated (Bernstein *et al.*, 1998). Parts of these terms are imaged on the second harmonic and may therefore interfere with the complex wave image of one displacement component in both SLIM-MRE methods. However, the ratio of the strength of the concomitant field over the field strength generated by an individual gradient is only on the order of 1% in small scale, high field scanners. Further, concomitant field effects in two scans with 180 degree mechanical phase shift cancel each other out in the phase-difference image, which is used for further processing (Klatt *et al.*, 2013). We note that conventional MRE is not affected by concomitant fields and that the baseline comparison (Table 1) results in similar error values for conventional MRE, SLIM-PC and SLIM-PV, which indicates that concomitant field effects do not impair MRE data when using multidirectional SLIM encoding.

MRE benefits from high spatial resolution and from full 3D wave field acquisition and inversion, which is independent of the orientation of the wave normal. Both SLIM-MRE approaches allow for the acquisition of three directions in 1/3 the time of conventional MRE and may therefore be powerful tools to increase the acceptance of 3D MRE acquisition schemes that are independent of the vibration transfer. SLIM-MRE is also less likely to suffer from motion errors by reducing the total time the specimen is being imaged in a stationary position by acquiring all vibration directions in a single scan. The only downside of SLIM acquisitions are reduced gradient amplitudes with the used Agilent MRI system, which are now distributed among 3 directions resulting in a loss of encoding efficiency.

6. Conclusion

This study assessed the feasibility of SLIM-MRE for in vivo mouse studies, and introduced an alternative SLIM method that encodes all three motion directions simultaneously without an increase in TE. Both methods show good agreement with the conventional MRE method. SLIM-PC compares to conventional MRE better than SLIM-PV in terms of the shear modulus maps, but requires an increase in TE. Finally, both methods show spatially averaged results that agree well with the ones obtained from conventional acquisitions. We will use SLIM-PC as our standard MRE approach for cerebral mouse applications and note that the SLIM-PV may be useful for clinical applications that use spatially averaged mechanical properties and where both measurement time and T2 relaxation are critical, such as human liver MRE.

References:

- Asbach P, Klatt D, Hamhaber U, Braun J, Somasundaram R, Hamm B and Sack I 2008 Assessment of liver viscoelasticity using multifrequency MR elastography *Magnetic Resonance in Medicine* **60** 373-9
- Bernstein M A, Zhou X J, Polzin J A, King K F, Ganin A, Pelc N J and Glover G H 1998 Concomitant gradient terms in phase contrast MR: analysis and correction *Magnetic resonance in medicine* **39** 300-8
- Boulet T, Kelso M L and Othman S F 2013 Long-Term In Vivo Imaging of Viscoelastic Properties of the Mouse Brain after Controlled Cortical Impact *Journal of Neurotrauma* **30** 1512-20
- Clayton E H, Garbow J R and Bayly P V 2011 Frequency-dependent viscoelastic parameters of mouse brain tissue estimated by MR elastography *Physics in Medicine and Biology* **56** 2391-406
- Daniel W W 2004 *Biostatistics: A Foundation for Analysis in the Health Sciences (8th Edition)*
- Elgeti T, Rump J, Hamhaber U, Papazoglou S, Hamm B, Braun J and Sack I 2008 Cardiac magnetic resonance elastography: initial results *Investigative radiology* **43** 762-72
- Freimann F B, Streitberger K J, Klatt D, Lin K, McLaughlin J, Braun J, Sprung C and Sack I 2012 Alteration of brain viscoelasticity after shunt treatment in normal pressure hydrocephalus *Neuroradiology* **54** 189-96
- Herzka D A, Kotys M S, Sinkus R, Pettigrew R I and Gharib A M 2009 Magnetic Resonance Elastography in the Liver at 3 Tesla Using a Second Harmonic Approach *Magnetic Resonance in Medicine* **62** 284-91
- Jamin Y, Boulton J K R, Li J, Popov S, Garteiser P, Ulloa J L, Cummings C, Box G, Eccles S A, Jones C, Waterton J C, Bamber J C, Sinkus R and Robinson S P 2015 Exploring the Biomechanical Properties of Brain Malignancies and Their Pathologic Determinants In Vivo with Magnetic Resonance Elastography *Cancer Research* **75** 1216-24

- Klatt D, Johnson C L and Magin R L 2015 Simultaneous, multidirectional acquisition of displacement fields in magnetic resonance elastography of the in vivo human brain *Journal of Magnetic Resonance Imaging* **42** 297-304
- Klatt D, Yasar T K, Royston T J and Magin R L 2013 Sample interval modulation for the simultaneous acquisition of displacement vector data in magnetic resonance elastography: theory and application *Physics in Medicine and Biology* **58** 8663-75
- Li S Y, Chen M, Wang W C, Zhao W F, Wang J Y, Zhao X N and Zhou C 2011 A feasibility study of MR elastography in the diagnosis of prostate cancer at 3.0T *Acta Radiologica* **52** 354-8
- Manduca A, Oliphant T E, Dresner M A, Mahowald J L, Kruse S A, Amromin E, Felmlee J P, Greenleaf J F and Ehman R L 2001 Magnetic resonance elastography: Non-invasive mapping of tissue elasticity *Medical Image Analysis* **5** 237-54
- Mariappan Y K, Glaser K J and Ehman R L 2010 Magnetic Resonance Elastography: A Review *Clinical Anatomy* **23** 497-511
- Mariappan Y K, Glaser K J, Hubmayr R D, Manduca A, Ehman R L and McGee K P 2011 MR elastography of human lung parenchyma: technical development, theoretical modeling and in vivo validation *Journal of Magnetic Resonance Imaging* **33** 1351-61
- McGarry M D J, Johnson C L, Sutton B P, Georgiadis J G, Van Houten E E W, Pattison A J, Weaver J B and Paulsen K D 2015 Suitability of poroelastic and viscoelastic mechanical models for high and low frequency MR elastography *Medical Physics* **42** 947-57
- McGarry M D J, Van Houten E E W, Johnson C L, Georgiadis J G, Sutton B P, Weaver J B and Paulsen K D 2012 Multiresolution MR elastography using nonlinear inversion *Medical Physics* **39** 6388-96
- Murphy M C, Curran G L, Glaser K J, Rossman P J, Huston J, Poduslo J F, Jack C R, Felmlee J P and Ehman R L 2012 Magnetic resonance elastography of the brain in a mouse model of Alzheimer's disease: initial results *Magnetic Resonance Imaging* **30** 535-9

- Murphy M C, Huston J, Jack C R, Glaser K J, Manduca A, Felmlee J P and Ehman R L 2011 Decreased Brain Stiffness in Alzheimer's Disease Determined by Magnetic Resonance Elastography *Journal of Magnetic Resonance Imaging* **34** 494-8
- Muthupillai R, Lomas D J, Rossman P J, Greenleaf J F, Manduca A and Ehman R L 1995 Magnetic resonance elastography by direct visualization of propagating acoustic strain waves *Science* **269** 1854-7
- Nir G, Sahebjavaher R S, Sinkus R and Salcudean S E 2015 A framework for optimization - based design of motion encoding in magnetic resonance elastography *Magnetic Resonance in Medicine* **73** 1514-25
- Oliphant T E, Manduca A, Ehman R L and Greenleaf J F 2001 Complex-valued stiffness reconstruction for magnetic resonance elastography by algebraic inversion of the differential equation *Magnetic Resonance in Medicine* **45** 299-310
- ReviseMRI.com 2017 http://www.reviseMRI.com/questions/equip_qa/measuring_snr.
- Rump J, Klatt D, Braun J, Warmuth C and Sack I 2007 Fractional encoding of harmonic motions in MR elastography *Magnetic Resonance in Medicine* **57** 388-95
- Sack I, Beierbach B, Hamhaber U, Klatt D and Braun A 2008 Non-invasive measurement of brain viscoelasticity using magnetic resonance elastography *Nmr in Biomedicine* **21** 265-71
- Sahebjavaher R S, Nir G, Gagnon L O, Ischia J, Jones E C, Chang S D, Yung A, Honarvar M, Fazli L, Goldenberg S L, Rohling R, Sinkus R, Kozlowski P and Salcudean S E 2015 MR elastography and diffusion-weighted imaging of ex vivo prostate cancer: quantitative comparison to histopathology *Nmr in Biomedicine* **28** 89-100
- Schregel K, née Tysiak E W, Garteiser P, Gemeinhardt I, Prozorovski T, Aktas O, Merz H, Petersen D, Wuerfel J and Sinkus R 2012 Demyelination reduces brain parenchymal stiffness quantified in vivo by magnetic resonance elastography *Proceedings of the National Academy of Sciences* **109** 6650-5

- Shi Y, Glaser K J, Venkatesh S K, Ben - Abraham E I and Ehman R L 2015 Feasibility of using 3D MR elastography to determine pancreatic stiffness in healthy volunteers *Journal of Magnetic Resonance Imaging* **41** 369-75
- Sinkus R, Tanter M, Xydeas T, Catheline S, Bercoff J and Fink M 2005 Viscoelastic shear properties of in vivo breast lesions measured by MR elastography *Magnetic resonance imaging* **23** 159-65
- Streitberger K J, Wiener E, Hoffmann J, Freimann F B, Klatt D, Braun J, Lin K, McLaughlin J, Sprung C, Klingebiel R and Sack I 2011 In vivo viscoelastic properties of the brain in normal pressure hydrocephalus *Nmr in Biomedicine* **24** 385-92
- Venkatesh S K, Yin M, Glockner J F, Takahashi N, Araoz P A, Talwalkar J A and Ehman R L 2008 Magnetic resonance elastography of liver tumors-preliminary results *AJR. American journal of roentgenology* **190** 1534
- Wuerfel J, Paul F, Beierbach B, Hamhaber U, Klatt D, Papazoglou S, Zipp F, Martus P, Braun J and Sack I 2010 MR-elastography reveals degradation of tissue integrity in multiple sclerosis *Neuroimage* **49** 2520-5
- Yin M, Talwalkar J A, Glaser K J, Manduca A, Grimm R C, Rossman P J, Fidler J L and Ehman R L 2007 Assessment of hepatic fibrosis with magnetic resonance elastography *Clinical Gastroenterology and Hepatology* **5** 1207-13
- Yin Z Y, Magin R L and Klatt D 2014 Simultaneous MR Elastography and Diffusion Acquisitions: Diffusion-MRE (dMRE) *Magnetic Resonance in Medicine* **71** 1682-8

Tables:

Table 1. Baseline comparison of follow-up experiments using repeated conventional, SLIM-PC, and SLIM-PV MRE scans. Listed are the Spearman's rank correlation values for the complete set of MRE images: curl wave images for each direction (Q_x , Q_y and Q_z) and the shear modulus maps for storage (G') and loss moduli (G'').

Image Type	Conventional	SLIM-PC	SLIM-PV
Q_x	0.97	0.79	0.96
Q_y	0.93	0.82	0.96
Q_z	0.94	0.97	0.97
G'	0.89	0.79	0.87
G''	0.87	0.78	0.83

Table 2. SNR of repeated baseline scans. For the conventional MRE scans, each scan requires three separate scans for every encoding direction, therefore there are 3 SNR values listed in the order read (Y-direction), phase (X-direction), and slice (Z-direction) directions.

Scan	SNR
Conventional 1	22.7, 13.0, 22.3
Conventional 2	23.6, 22.6, 21.0
SLIM-PC 1	23.6
SLIM-PC 2	23.2
SLIM-PV 1	24.0
SLIM-PV 2	23.5

Table 3. Spearman’s rank correlation for all mice, both SLIM methods, curled wave field for each direction. The final column is the mean of all mice for the corresponding row.

Method	Q_n	M1	M2	M3	M4	M5	M6	Mean
SLIM-PC	Q _x	0.80	0.87	0.93	0.91	0.79	0.82	0.85
	Q _y	0.53	0.84	0.90	0.90	0.82	0.72	0.79
	Q _z	0.71	0.87	0.93	0.96	0.92	0.80	0.86
SLIM-PV	Q _x	0.63	0.64	0.62	0.68	0.65	0.73	0.66
	Q _y	0.26	0.64	0.64	0.72	0.65	0.54	0.58
	Q _z	0.45	0.75	0.81	0.87	0.78	0.64	0.71

Table 4. Spearman’s rank correlation for the complex shear modulus images (G^*) obtained using SLIM-PC and SLIM-PV. G' and G'' represent the shear storage and loss moduli, respectively. The last column is the mean of all errors for all mice.

Method	G^*	M1	M2	M3	M4	M5	M6	Mean
SLIM-PC	G'	0.7	0.8	0.8	0.9	0.9	0.7	0.80
	G''	0.7	0.8	0.8	0.8	0.8	0.7	0.76
SLIM-PV	G'	0.6	0.7	0.8	0.8	0.8	0.7	0.73
	G''	0.6	0.7	0.7	0.7	0.7	0.7	0.69

Table 5. Spatially averaged shear modulus values for each mouse and method. All units are in kPa.

Method	G*	M1	M2	M3	M4	M5	M6	Mean
CONVENTIONAL	G'	4.88	5.62	6.21	6.72	7.23	4.91	5.93
	G''	2.38	2.84	3.27	3.23	3.54	2.44	2.95
SLIM-PC	G'	4.91	5.40	6.21	7.17	7.07	5.28	6.01
	G''	2.34	2.75	3.29	3.62	3.52	3.00	3.09
SLIM-PV	G'	4.79	5.29	5.95	6.85	6.85	5.11	5.81
	G''	2.36	2.76	3.20	3.60	3.67	2.92	3.09

Figures:

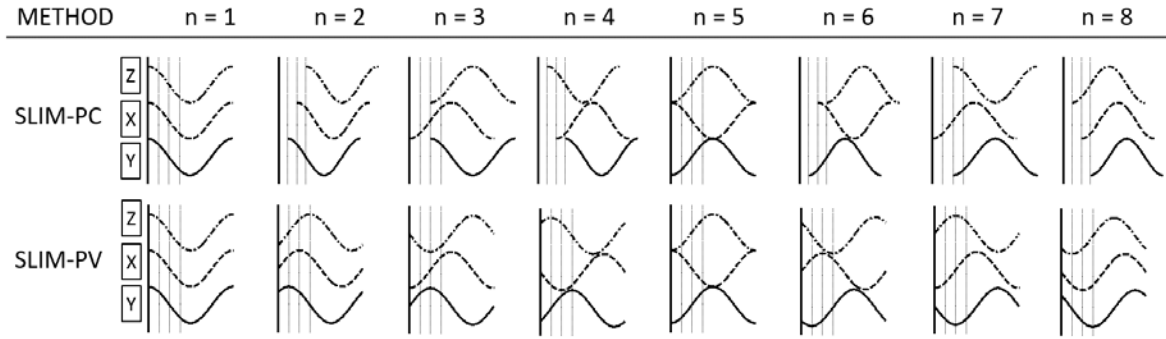


Figure 1. Comparison of SLIM methods based on varying either the start time (SLIM-PC) or the phase (SLIM-PV) of the MEG shape. Each column represents a time step ($n = [1:8]$), which corresponds to a specific mechanical phase, and each row the SLIM method with the MEG shape for each Cartesian direction. The solid black vertical line represents the common start time for the MEG shape for all time steps. Each dotted vertical line represents $1/8$ of the MEG period. Note, for SLIM-PC, to reduce the impact of TE time increase, we make use of the periodicity of harmonic functions and the fact that sign flips correspond to 180° phase shifts.

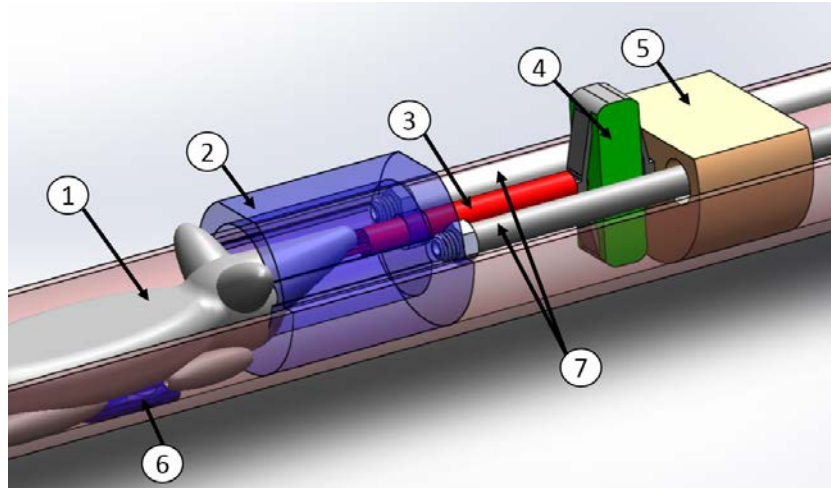


Figure 2. Bite bar actuator and anesthesia setup for MRE imaging. 1) Approximate mouse representation, 2) retractable nose cone, 3) bite bar, 4) piezo actuator, 5) piezo attachment base, 6) respiration pillow sensor, 7) outlet and inlet anesthesia lines.

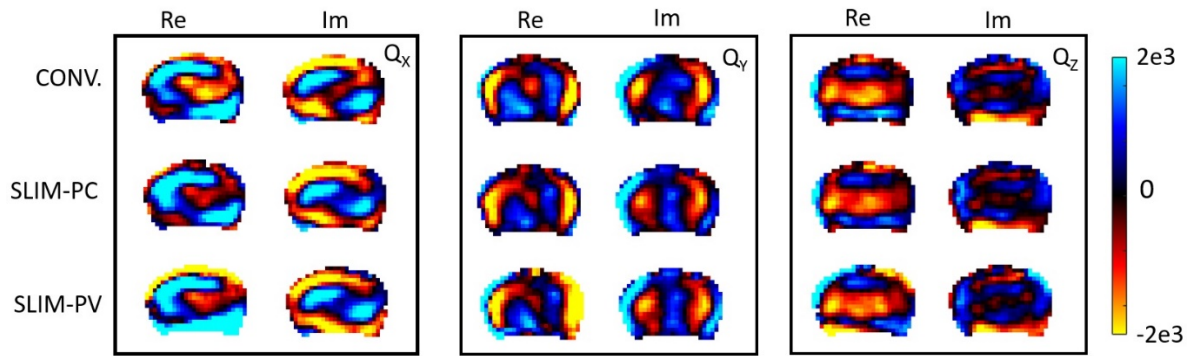


Figure 3. Comparison of the complex wave image after application of the curl for conventional MRE and SLIM-MRE methods. Conventional MRE images are along the top row, SLIM-PC images along the 2nd row, and SLIM-PV images along the bottom row. Each set of images inside the boxes represent a central slice of mouse 5 for each Cartesian direction (Q_x , Q_y , and Q_z). Also, the real and imaginary part is shown side by side. The curled wave data is dimensionless.

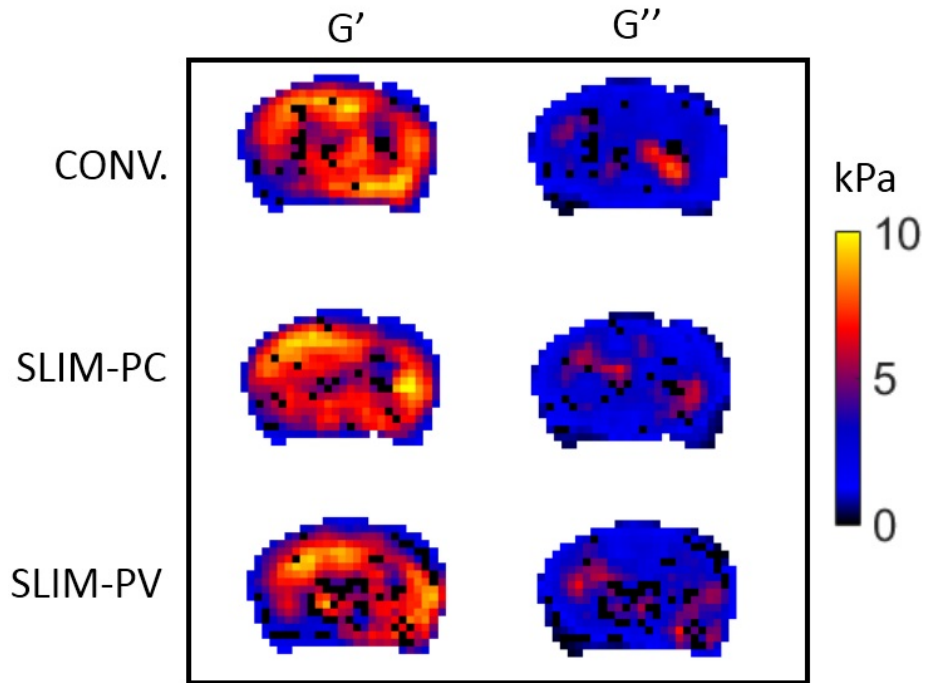


Figure 4. Comparison of the complex shear modulus images of conventional MRE and SLIM-MRE methods for a single central slice of mouse 5. The columns from left to right represent the shear storage and loss moduli, respectively, and the rows designate the MRE method used. The black points represent rejected pixels based on a shear modulus threshold of >30 kPa or < 50 Pa, and were not included in correlation calculations.

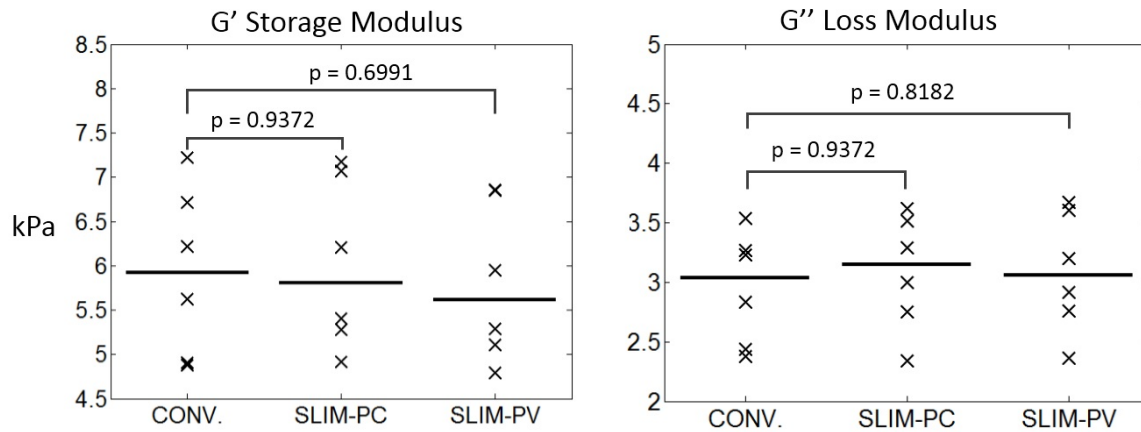


Figure 5. The pair wise Wilcoxon rank sum test scatter plots. Spatially averaged shear moduli obtained using each SLIM method are compared to the ones obtained using conventional acquisitions (see also Table 4) and the corresponding p-values are shown with brackets across groups. The dark line represents the inter-individual median and the storage modulus is shown in the left graph with the loss modulus on the right. No statistically significant differences were found between the groups.